

# Catalysis Science & Technology

Accepted Manuscript

This article can be cited before page numbers have been issued, to do this please use: Y. Liu, Z. Tang, Y. Yu, W. Liu, Z. chen, R. Wang, H. Liu, H. Wu and M. Y. He, *Catal. Sci. Technol.*, 2020, DOI: 10.1039/D0CY00126K.



This is an Accepted Manuscript, which has been through the Royal Society of Chemistry peer review process and has been accepted for publication.

Accepted Manuscripts are published online shortly after acceptance, before technical editing, formatting and proof reading. Using this free service, authors can make their results available to the community, in citable form, before we publish the edited article. We will replace this Accepted Manuscript with the edited and formatted Advance Article as soon as it is available.

You can find more information about Accepted Manuscripts in the [Information for Authors](#).

Please note that technical editing may introduce minor changes to the text and/or graphics, which may alter content. The journal's standard [Terms & Conditions](#) and the [Ethical guidelines](#) still apply. In no event shall the Royal Society of Chemistry be held responsible for any errors or omissions in this Accepted Manuscript or any consequences arising from the use of any information it contains.

## ARTICLE

**Deboronation-assisted construction of defective Ti(OSi)<sub>3</sub>OH species in MWW-type titanosilicate and their enhanced catalytic performance**Received 00th January 20xx,  
Accepted 00th January 20xx

DOI: 10.1039/x0xx00000x

Zhimou Tang<sup>a</sup>, Yunkai Yu<sup>a</sup>, Wei Liu<sup>b</sup>, Zhen Chen<sup>a</sup>, Rui Wang<sup>a</sup>, Haoxin Liu<sup>a</sup>, Haihong Wu<sup>a</sup>, Yueming Liu<sup>\*a</sup> and Mingyuan He<sup>a</sup>

A thorough investigation towards the nature of the Ti species in the boron-containing Ti-MWW zeolite has been carried out. It is found that the inactive extra-framework TiO<sub>6</sub> species could cover up the zeolite Lewis-acid property, through the weak interaction between the “Ti(IV)” atom and “O” atom (TiO<sub>6</sub> species). The nitric acid treatment could remove these TiO<sub>6</sub> species easily off the as-synthesized Ti-MWW(P), followed by the exposure of zeolite Lewis acid. Importantly, the formation of new Ti(OSi<sub>3</sub>)OH species, with the strong Lewis-acid strength, is facilitated in the modification process. Thereby, the modified Ti-MWW zeolite performed an improved catalytic activity in alkene epoxidation reactions. The removal of framework B(IV) species around TiO<sub>4</sub> species is an essential step because it could accelerate the transformation of perfect Ti(OSi)<sub>4</sub> species to defective Ti(OSi<sub>3</sub>)OH species in zeolites. Moreover, the strategy to construct Ti(OSi)<sub>3</sub>OH species was also applied successfully in boron-containing Ti-MCM-56 zeolites. Considering the active specie environment can be modulated effectively with the removal of framework tetra-coordinate boron, this strategy can also be beneficial for the preparation of other high-performance titanosilicates.

**1. Introduction**

Green chemistry motivates the manufacturers to pay attention to eradicate pollution by minimizing or eliminating the hazards of chemical feedstocks, reagents, solvents, and products<sup>1</sup>. As a milestone in the field of zeolite catalysis, the titanium silicalites-1/H<sub>2</sub>O<sub>2</sub> (TS-1/H<sub>2</sub>O<sub>2</sub>) catalytic system has set off veritable revolutions in the synthesis of high-value chemicals, because these processes are environmentally benign in terms of greenness and zero waste disposal, in other words, these reactions give water as the sole byproduct<sup>2-5</sup>. Great efforts, focusing on the design and development of high-performance titanosilicates, such as Ti-MOR, Ti-Beta, and Ti-MWW zeolite, have therefore been devoted by both the academic and industrial circles<sup>6-9</sup>.

As for Ti-MWW zeolite, it possesses a unique pore structure of 12-MR side cups on the crystallites exterior as well as two independent 10-MR channel systems; one contains 12-MR supercages and the other is of sinusoidal tortuosity<sup>10</sup>. And the theoretical analyses and experimental tests have jointly

elucidated its peculiarities relative to the other titanosilicate in the catalytic performance and preparation method<sup>11-13</sup>. Ti-MWW zeolite not only showed high activity in the selective epoxidation of propylene, allyl chloride (ALC), allyl alcohol (AAL), and diallylether, but also exhibited excellent selectivity in the ammoxidation of methyl ethyl ketone (MEK) and cyclohexanone<sup>14-17</sup>. However, it is difficult to obtain Ti-MWW from the synthetic gels containing only silicon and titanium via hydrothermal synthesis methods, and thus post-synthesis method is always an alternative<sup>18</sup>. The breakthrough in the hydrothermal synthesis of Ti-MWW zeolite with high crystallinity is the introduction of boric acid<sup>9</sup>, which is based on the synthesis of B-containing MWW zeolite ERB-1<sup>19</sup>. Though the incorporation of Ti species into MWW framework with the assistance of boric acid, it has been found that acid treatment was an absolutely necessary process to get the final Ti-MWW zeolite with the catalytic ability<sup>13, 20, 21</sup>. They have mentioned that acid treatment was applied to extract non-framework TiO<sub>6</sub> species, which deposited on the surface of MWW layers and caused a negative effect in epoxidation reactions. Yet, it should be noticed that the acid treatment could change the micro-environment of Ti active species including the structure of framework Ti active species, which could also influence zeolite catalytic performance<sup>11</sup>. Some researchers indicated that a part of non-framework TiO<sub>6</sub> species could be converted into the framework Ti active species in the acid treatment process<sup>22, 23</sup>, whereas studies have already suggested that the loss of “Ti” species, instead of the reinsertion, could be more likely to occur

<sup>a</sup> Shanghai Key Laboratory of Green Chemistry and Chemical Processes, School of Chemistry and Molecular Engineering, East China Normal University, North Zhongshan Rd. 3663, Shanghai 200062, P. R. China

<sup>b</sup> Shanghai Research Institute of Petrochemical Technology, SINOPEC, North Pudong Rd. 1658, Shanghai 201208, P. R. China.

\*E-mail: [ymliu@chem.ecnu.edu.cn](mailto:ymliu@chem.ecnu.edu.cn)

Electronic Supplementary Information (ESI) available: [details of any supplementary information available should be included here]. See DOI: 10.1039/x0xx00000x

under this serious acidic condition<sup>13</sup>. Actually, an important factor needs to be considered, which is concerned with the behaviours of boron species in the treatment process. It was explained that boric acid could serve as the structure-supporting agent in the synthesis of Ti-MWW zeolite, and assist the incorporation of Ti atoms into the MWW framework<sup>13,24,25</sup>. Besides, the oxidation activity of Ti-MWW zeolite could indeed be influenced by boron species<sup>26</sup>. Hence, the true effects of the acid treatment on zeolite property is still a mystery. These questions drive people to search for the fact, which involves many factors including the change of active Ti states and alterations of zeolite acidic properties and catalytic abilities.

It's widely accepted that framework Ti species in titanosilicates serve as the active sites, because their Lewis acidity could act as a trigger point in the activation of H<sub>2</sub>O<sub>2</sub>, which is a critical step in Ti-catalyzed reactions with H<sub>2</sub>O<sub>2</sub> as the oxidant<sup>11,27,28</sup>. Collectively, a series of Ti active species in titanosilicates has been reported<sup>29-33</sup>. The Lewis acid strength is increased in F-Ti-MWW<sup>34</sup> and TS-1<sup>5</sup> zeolite<sup>35</sup>, which arise from the electron-withdrawing effect of F in the vicinity of Ti active sites, and the more positive charge of Ti atom in Ti(OSi)<sub>3</sub>OH species respectively. Due to the superior ability to activate H<sub>2</sub>O<sub>2</sub>, the expansion of the coordination number of Ti atoms ("TiO<sub>5</sub>" and "TiO<sub>6</sub>" species) in zeolites could also result in an improved catalytic activity<sup>36-38</sup>. The above analysis could be instructive for us to explore the active species in Ti-MWW zeolite.

Herein, a comprehensive investigation was carried out to make certain the structure of Ti active centres and its formation process in conventional boron-containing Ti-MWW. Results revealed that the acid treatment could remove easily the inactive extraframework "TiO<sub>6</sub>" species, and framework Ti(OSi)<sub>4</sub> active species are therefore exposed. The removal of framework B(IV) species in the acidic environment is accompanied by the desilication around Ti(OSi)<sub>4</sub> species, facilitating the formation of defective Ti(OSi)<sub>3</sub>OH species. The Lewis-acid strength of zeolite could therefore be enhanced, which is beneficial for the improvements of catalytic oxidation activity. Moreover, this method has also helped us prepare the Ti-MCM-56 zeolite with improved catalytic performance, which indicates that B(IV) species could not only help the incorporation of Ti atoms into zeolite skeleton, but also play an important role in building the unique Ti active species in titanosilicates. These explorations will be of great guidance for the development of Ti-MWW zeolite-based industrial catalysts, and may especially provide the path for designing highly efficient titanosilicate catalysts

## 2. Experimental Section

### 2.1 Catalyst preparation

Ti-MWW lamellar precursor (Ti-MWW(P)) was synthesized in a boric acid system with piperidine (PI) as structure-directing agent (SDA), following previously reported methods<sup>13</sup>. The starting gels with the molar compositions of 1.0 SiO<sub>2</sub>: (0.0167 or

0.04) TiO<sub>2</sub>:1.4 PI:0.67 B<sub>2</sub>O<sub>3</sub>:19 H<sub>2</sub>O were crystallized in a 100 mL Teflon-lined autoclave under rotation (100 rpm) at 443 K for 7 days. The direct calcination with Ti-MWW(P) (Si/Ti=25) resulted in Ti-MWW(P)-C sample. The nitric acid treatment could be applied to Ti-MWW(P) sample. If the acid-treated time was controlled, the Ti-MWW(P)-AT-x samples could be synthesized, where x (x = 2, 4, 8, 12, 16 and 24) represents the hours of treatment time. For example, the preparation of Ti-MWW(P)-AT-24 is that Ti-MWW(P) (Si/Ti=25) is treated with 2.0 M HNO<sub>3</sub> for 24 h at a solid-to-liquid weight ratio of 1:50 under the refluxed conditions (105°C). All acid-treated samples were further calcined in air at 823 K for 8 h to obtain the products.

Ti-MWW sample with a large quantity of boron species (labeled as Ti-MWW-(B)) was prepared using a previously published procedure<sup>34</sup>. The Ti-MWW(P) (Si/Ti=25) was treated with 3.0 M HNO<sub>3</sub> for 24 h at a solid-to-liquid weight ratio of 1:50 at the room temperature with the addition of the NH<sub>4</sub>F (Si/F=128). The acid-treated sample was further calcined in air at 823 K for 8 h to obtain the product Ti-MWW-(B).

The Ti-MCM-56 zeolite was prepared following previously reported methods<sup>39</sup>. Ti-MWW(P) (Si/Ti=25) is treated using 1.0 M HNO<sub>3</sub> for 24 h at a solid-to-liquid weight ratio of 1:50 at the room temperature. The acid-treated sample was further calcined in air at 823 K for 8 h to obtain the product Ti-MCM-56. The modified Ti-MCM-56 zeolite was synthesized, through the addition of mixture at a PI/SiO<sub>2</sub> molar ratio of 1.0 and an H<sub>2</sub>O/SiO<sub>2</sub> molar ratio of 10 at 443 K for 24 h. The resulting solid was collected by filtration, washed with deionized water and dried at 373 K overnight to obtain the Re-Ti-MCM-56(P) zeolite. Furtherly, the Ti-MCM-56 and Re-Ti-MCM-56(P) samples were treated with 0.5 M HNO<sub>3</sub> at a solid-to-liquid weight ratio of 1:30 for 20 h under the refluxed condition. The treated samples were further calcined in air at 823 K for 8 h to obtain the products, which were named as Ti-MCM-56-AT-C and Re-Ti-MCM-56(P)-AT-C sample respectively.

### 2.2 Catalysts characterization

The synthesized samples were characterized by the X-ray diffraction (XRD) on a Rigaku Ultima IV diffractometer (Cu-K $\alpha$ ), by inductively coupled plasma (ICP) on a Thermo IRIS Intrepid II XSP atomic emission spectrometer, by N<sub>2</sub> adsorption (BEL-MAX instrument), by scanning electron microscopy (Hitachi S-4800), and by UV-visible (Shimadzu 2700 PC) and IR (Nicolet Nexus 670 FT-IR spectrometer). For pyridine spectra measurement (1000-4000 cm<sup>-1</sup>), a self-supported wafer (9.6 mg·cm<sup>-1</sup> thickness and 2 cm in diameter) was set in a quartz IR cell sealed with CaF<sub>2</sub> windows connected with a vacuum system (Py-IR). After the sample was evacuated at 723 K for 1 h, the pyridine adsorption was carried out by exposing the wafer to pyridine vapor (1.3 kPa) at 298 K for 20 min. The physisorbed and chemisorbed pyridine was then removed by evacuation at different temperatures (323 K-523 K) for 0.5 h. All of the spectra were collected at room temperature. <sup>29</sup>Si solid-state MAS NMR spectra were recorded on a VARIAN VNMR5-400WB spectrometer under a one-pulse condition with a frequency of 79.43 MHz, a spinning rate of 3000 rps, and a recycling delay of 60 s, the chemical shift was referred to Q8M8([(CH<sub>3</sub>)<sub>3</sub>SiO]<sub>8</sub>-

SiO<sub>12</sub>). <sup>11</sup>B NMR and spectra were recorded with a frequency of 128.27 MHz, a spinning rate of 9.0 kHz, and a recycling delay of 5 s. NaBH<sub>4</sub> was used as the reference for chemical shift. UV Raman spectra were recorded on UV-RAMAN100 Raman spectrometer made by Beijing ZOLIX INSTRUMENTS CO. LTD. A 244-nm line of a LEXEL laser of a He-Gd laser were used as the excitation sources. The X-ray photoelectron spectra (XPS) were acquired with a Thermo Scientific ESCALAB250xi instrument using X-Ray Monochromatisation and operating at a constant power of 200 W.

## 2.3 Catalysts testing

### 2.3.1 The epoxidation reaction of 1-hexene/chloropropene/cyclopentene/propylene

The epoxidation of 1-hexene/chloropropene/cyclopentene were carried out at 333 K for 2 h in a 50 mL round-bottomed flask equipped with a reflux condenser. In a typical reaction, 50 mg of catalyst, 10 mL of CH<sub>3</sub>CN, 10 mmol of 1-hexene/chloropropene/cyclopentene, and 10 mmol of H<sub>2</sub>O<sub>2</sub> aqueous solution (30 wt.%) under vigorous stirring. The product was analyzed on an Agilent GC-7890A gas chromatograph equipped with a DB-WAX capillary column (30 m × 320 μm × 0.25 μm) and an FID detector using cyclohexanone as an internal standard. The residual free H<sub>2</sub>O<sub>2</sub> was determined by the titration method with 0.05 M Ce(SO<sub>4</sub>)<sub>2</sub> solution.

The epoxidation of propylene with H<sub>2</sub>O<sub>2</sub> was carried out in a stainless steel reactor that was immersed in a bath controlled at the required temperature. In a typical run, the mixture containing 100 mg of catalyst, 25 mL of CH<sub>3</sub>CN, 30 mmol of H<sub>2</sub>O<sub>2</sub> aqueous solution (30 wt.%) were loaded into the reactor. Then propylene was charged at constant pressure (0.4 MPa) and the mixture was heated at 323 K under magnetic agitation for 50 min. The reactive product was analyzed on an Agilent GC-7890A gas chromatograph equipped with a DB-WAX capillary column (30 m × 320 μm × 0.25 μm) by using 0.50 g of toluene as internal standard, and the unconverted H<sub>2</sub>O<sub>2</sub> was calculated by titration with 0.05 M Ce(SO<sub>4</sub>)<sub>2</sub> solution.

### 2.3.2 The cyclohexanone ammoximation reaction

In a typical run, a 50-mL three-neck flask reactor equipped with a magnetic stirrer and a condenser was used as batch wise reactor, after loading 150 mg of catalyst, 10 mmol of cyclohexanone, 17 mmol of aqueous NH<sub>3</sub>-solution (25 wt.%), 5000 mg of solvent (H<sub>2</sub>O/*t*-BuOH co-solvent with a weight ratio of 0.15:0.85). Then the reaction mixture was vigorously stirred, and when the temperature raised to the desire value (335 K), the reaction was initiated by adding 11 mmol H<sub>2</sub>O<sub>2</sub> aqueous solution (30 wt.%) continuously at a constant rate (4 g·h<sup>-1</sup>) with a micro pump. It was worth noting that the small amount of high concentrations of H<sub>2</sub>O<sub>2</sub> (30 wt.%) was diluted into 5000 mg by solvent firstly before adding aimed at controlling the accuracy of feeding speed and avoiding introducing too much water into the reaction system if using the high concentration of H<sub>2</sub>O<sub>2</sub> directly. After finishing H<sub>2</sub>O<sub>2</sub> addition within 1.5 h, the mixture was further reacted for another 0.5 h. The catalyst solid was removed by centrifuging and then the product was analyzed and quantified on an Agilent GC-7890A gas chromatograph

equipped with a DB-WAX capillary column (30 m × 320 μm × 0.25 μm) and an FID detector. DOI: 10.1039/D0CY00126K

### 2.3.3 The alcoholysis reaction of propylene oxide (PO)

The solvolysis of PO was carried out in a 50 mL round-bottomed flask equipped with a reflux condenser. In a typical run, 100 mg of catalyst, 10 mL of solvent (methanol), and 10 mmol of PO were added into the flask and reacted under vigorous stirring at 333 K for 2 h. The catalyst solid was removed by centrifuging and the product was analyzed and quantified on an Agilent GC-7890A gas chromatograph equipped with a DB-WAX capillary column (30 m × 320 μm × 0.25 μm) and an FID detector.

## 3. Results and discussion

### 3.1 The state of Ti active species in Ti-MWW zeolites

To find out the crucial changes during the whole process of acid treatment, the basic physicochemical properties among Ti-MWW(P), Ti-MWW(P)-C and Ti-MWW(P)-AT-24 samples were investigated firstly. Fig. 1A shows XRD patterns of the aforementioned samples. Both the well-crystallized Ti-MWW(P)-C and Ti-MWW(P)-AT-24 samples with the typical three-dimensional MWW topology were prepared through the transformations from the 2D lamellar Ti-MWW(P) sample, as characteristic diffraction peaks of (001) and (002) peaks at 2θ=3-7° disappeared, and other peaks related with the crystalline sheets parallel to ab-planes remained practically unchanged<sup>40</sup>. N<sub>2</sub> adsorption-desorption isotherms and BET calculations of Ti-MWW(P)-C and Ti-MWW(P)-AT-24 samples (Fig. 1B and Table 1) could reflect furtherly the integrity of pore structure and almost the same pore volume, which indicated that there is sufficient diffusion space for substrates to approach the Ti active sites. Combined with SEM images shown in Fig. S1, the representative morphology of thin hexagonal plates, stacking disorderly with the thickness around 50 nm and approximate 100 nm length, are observed in both the samples. The absence of impurities could also demonstrate the high crystallinity of these samples, which is in consistent with the results from XRD and BET measurements.

Due to its significant effect on the catalytic performance, the state of titanium species is always the primary consideration of researchers. UV-Vis spectroscopy is the commonly accepted method<sup>11, 41</sup>. A broad band projected at ca. 260 nm together with a weak shoulder band around ca. 210 nm, which are

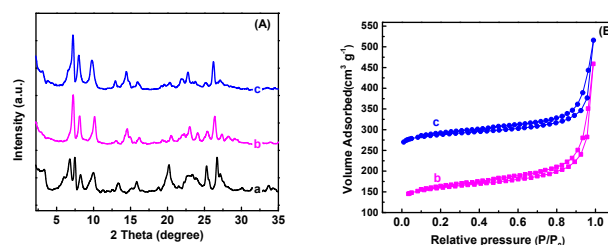
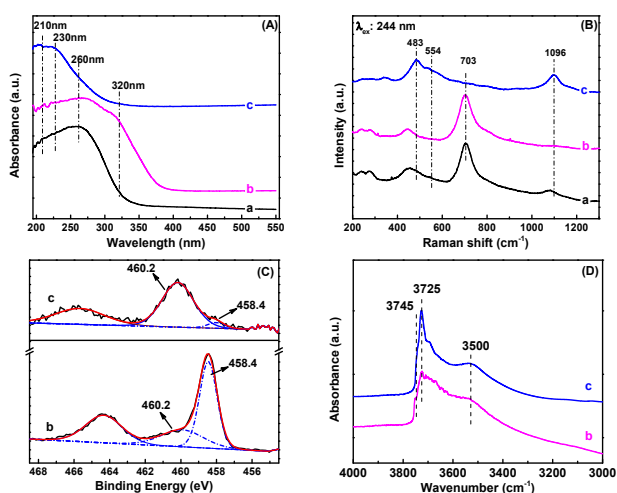


Fig. 1 Powder XRD patterns (A) and N<sub>2</sub> adsorption-desorption isotherms at 77 K (B) of Ti-MWW(P) (a), Ti-MWW(P)-C (b), and Ti-MWW(P)-AT-24 (c) samples. N<sub>2</sub> adsorption-desorption isotherms of Ti-MWW(P)-AT-24 (c) sample was lifted upward 150 units for comparison.



**Fig. 2** UV-Vis spectra (A), 244-nm excited UV resonance Raman spectra (B), Ti 2p XPS spectra (C), and IR spectra in the hydroxyl stretching evacuated at 723 K in the range of 1500-4000 cm<sup>-1</sup> (D) of Ti-MWW(P) (a), Ti-MWW(P)-C (b), and Ti-MWW(P)-AT-24 (c) samples.

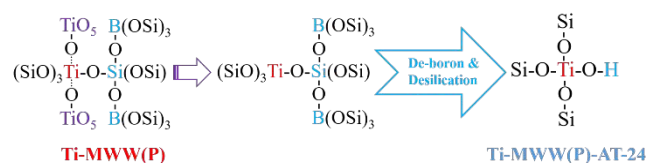
assigned to the “TiO<sub>6</sub>” and “TiO<sub>4</sub>” species respectively<sup>11</sup>, are found for Ti-MWW(P) (Fig. 2A(a)). For Ti-MWW(P)-C sample, a new band at ca. 330 nm appears (Fig. 2A(b)), which is a result of the formed anatase phase via the partial condensation and aggregation of neighbouring surface Ti species<sup>13</sup>. Unlike the framework “TiO<sub>6</sub>” species with piperidine/water molecule as a ligand<sup>42</sup>, the main band at ca. 260 nm of Ti-MWW(P) and Ti-MWW(P)-C is ascribed to the extra-framework six-coordinated Ti species<sup>42</sup>. This classification can be demonstrated, because these extra-framework Ti species are vulnerable to the acid treatment. As a consequence, the Ti-MWW(P)-AT-24 sample owns the band at ca. 230 nm after the treatment (Fig. 2A(c)). Based on the reports<sup>11, 22, 35</sup>, the red shift in UV-Vis spectra from 210 nm to 230 nm results from the difference in the Ti structure, that is, the transformation from the tetrapodal Ti(OSi)<sub>4</sub> to tripodal Ti(OSi)<sub>3</sub>OH species has occurred. Hence, the difference between the active sites could be visualized for the Ti-MWW(P)-C and Ti-MWW(P)-AT-24 sample. For one thing, Ti species of these samples have their individual characters (Fig. 2A), and for another, the content of Ti species is different because the Si/Ti ratio is 29 for Ti-MWW(P)-C, and 44 for Ti-MWW(P)-AT-24 samples respectively (Table 1).

UV-Raman technology was applied to find the delicate difference of Ti species in the samples. As the 244 nm laser excited in UV-Raman spectra is relatively close to the UV-Vis wavelength of the “TiO<sub>6</sub>” (260-280 nm) and “TiO<sub>4</sub>” species (210-230 nm), the resonance enhancement of absorption bands of corresponding Ti species are deduced to be prominent<sup>37</sup>. Thus, a sharp absorption band centred at ~700 cm<sup>-1</sup> in UV-Raman spectra could be observed when amorphous “TiO<sub>6</sub>” species are generated in titanosilicates<sup>38, 43</sup>. Raman characterizations of Ti-MWW(P) and Ti-MWW(P)-C display a dominant band at 703 cm<sup>-1</sup> in the 244 nm laser excitation (Fig. 2B(a, b)), which were in line with the UV-Vis analysis. The extremely weak band at ~1100 cm<sup>-1</sup>, a symbol of “TiO<sub>4</sub>” species<sup>43</sup>, was also observed. Although the recent workers<sup>22, 23</sup> suggested that framework “TiO<sub>4</sub>” species in Ti-MWW(P) zeolite were extremely traced, and therefore the

near disappearance at ~1100 cm<sup>-1</sup> Raman band seems to be reasonable. Yet, it still confuses us about the few incorporations of Ti atoms into the crystallographic locations of the MWW structure in the synthesis process. Another factor should be taken into consideration. The extraframework “TiO<sub>6</sub>” species are widely dispersed on the large external surface of the lamellar MWW precursor, which could thereby cover up the “TiO<sub>4</sub>” species. The speculation could be verified via the characterizations of the Ti-MWW(P)-AT-24 sample. As expected, Raman bands at 483, 554, 1096, and 348 cm<sup>-1</sup>, attributed to bending, symmetric and asymmetric stretching vibrations of framework “TiO<sub>4</sub>” species, and the MWW structure units respectively<sup>44-46</sup>, appeared when the extraframework “TiO<sub>6</sub>” species are removed from Ti-MWW(P) zeolite (Fig. 2B(c)).

As another effective method, the X-ray photoelectron spectroscopy (XPS) is usually used to observe the state of Ti species on the surface of zeolite because of the connections between the Ti binding energy (BE) and charge of Ti atoms. The Ti 2p<sub>3/2</sub> band at the binding energy of 460.2 eV is assigned to the Ti ions in the tetrahedral coordination state (Ti(IV) species), and the shoulder Ti 2p<sub>3/2</sub> band observed at 458.4 eV is the characteristic of Ti species existing in the form of octahedral coordinated Ti species (Ti(VI) species)<sup>47</sup>. Both bands are observed in Ti-MWW(P)-C and Ti-MWW(P)-AT-24 sample (Fig. 2C). The existence of the framework Ti(IV) in the Ti-MWW(P)-C sample could therefore be determined, which is in consistent with the UV-Vis measurements (Fig. 2C(b)). Meanwhile, the major peak at 458.4 eV found for Ti-MWW(P)-C sample also suggests that there are so large amounts of TiO<sub>6</sub> species that framework Ti(IV) species could be concealed (Fig. 2C(b)). Hence, the varieties of Ti species in Ti-MWW zeolite prompted us to proceed the deeper researches.

IR spectroscopy is effective to identify the zeolite surface acidity influenced by the surface structural OH, and authenticate the Lewis/Brønsted acid type originated from the various heteroatoms<sup>11, 48, 49</sup>. Fig. 2D shows the IR spectra in the OH vibration regions. Bands at 3745, 3725, and 3500 cm<sup>-1</sup>, assigned to the terminal silanols, internal hydroxyl-bonded silanols, and silanol nests respectively<sup>50-52</sup>, are found for the Ti-MWW(P)-C and Ti-MWW(P)-AT-24 sample. The 3676 cm<sup>-1</sup> band, once ascribed to the titanol groups, is not evident, which is probably because the stretching of Ti-OH group is far less intense than silanol groups, or its vibration mode do not give a sharp enough band to be observable<sup>34, 52</sup>. Apart from the band at 3500 cm<sup>-1</sup>, Ti-MWW(P)-AT-24 sample shows a more intense band at 3725 cm<sup>-1</sup> than that in Ti-MWW(P)-C sample (Fig. 2D), which means more Si-OH(Si) and Si-OH(Ti) species are present in the former<sup>52-54</sup>. Solid <sup>29</sup>Si MAS NMR results could also explain



**Scheme 1** A possible schematic diagram for the evolution of titanium species in Ti-MWW zeolite during the acid treatment.

this standpoint (Fig. S2). It is known that the fraction of Si atoms coordinated to -OH groups (i.e., Si-OH) within the sample could be estimated, based on their distinct NMR features at chemical shifts of -90, -100 ppm, and the region of -105 to -130 ppm on zeolites. Features at -90 and -100 ppm, corresponding to Si atoms that possess the hydroxyl moiety (i.e., Si(OSi)<sub>2</sub>(OH)<sub>2</sub> and Si(OSi)<sub>3</sub>(OH), are denoted as Q<sup>2</sup> and Q<sup>3</sup> respectively<sup>55, 56</sup>. Peaks in the region of -105 to -130 ppm originate from Si atoms coordinated to four siloxane functions (i.e., Si(OSi)<sub>4</sub>, denoted as Q<sup>4</sup> sites). Compared with the Ti-MWW(P)-C sample, the higher ratio of Q<sup>2</sup> and Q<sup>3</sup> was confirmed in Ti-MWW(P)-AT-24 sample (Fig. S2), which indicates the more Ti-OH sites in the acid-treated sample are possibly present.

Based on FT-IR spectra in the pyridine vibration region after pyridine absorption and desorption at different temperatures on samples, the acid property could be identified. The infrared absorption at 1580 and 1446 cm<sup>-1</sup> are attributed to pyridine species bonded to Lewis acidic sites, while the band at 1540 cm<sup>-1</sup> is assigned to the pyridinium ion<sup>12, 57</sup>. It is observed that the 1446 cm<sup>-1</sup> band is absent for Ti-MWW(P) sample (Fig. S3A), indicating that the Lewis acid of Ti(IV) species has been covered up by the widely dispersed "TiO<sub>6</sub>" species, which is in consistent with the UV-Raman spectra. The effect on Ti(IV) could also be demonstrated by the appearance of 1446 cm<sup>-1</sup> band with the Ti-MWW(P)-AT-24 sample after the removal of extraframework "TiO<sub>6</sub>" species in the process of acid treatment (Fig. S3B). It should be mentioned that the baseline goes upward for Ti-MWW(P)-C sample in the region of over 1500 cm<sup>-1</sup>, which originates from the effect of Si-O-B stretching vibration (around 1400 cm<sup>-1</sup>)<sup>26</sup>.

Finally, the state of Ti species with these Ti-MWW samples could be figured out (Scheme 1). The extraframework "TiO<sub>6</sub>" species could combine with "TiO<sub>4</sub>" species in a manner of the weak interactions between the "Ti(IV)" and "O" atom (TiO<sub>6</sub> species). Therefore, the Lewis-acid property of the framework Ti(IV) vanish in Ti-MWW(P)-C sample. Synchronously, UV-Vis

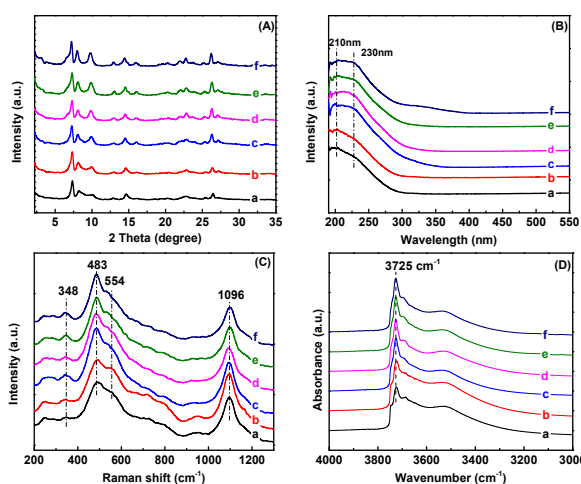


**Fig. 3** Powder XRD patterns (A), UV-Vis spectra (B), the 244-nm excited UV resonance Raman spectra (C), and IR spectra in the hydroxyl stretching evacuated at 723 K in the range of 1500-4000 cm<sup>-1</sup> (D) of Ti-MWW(P)-AT-x samples: (a) Ti-MWW(P)-AT-2, (b) Ti-MWW(P)-AT-4, (c) Ti-MWW(P)-AT-8, (d) Ti-MWW(P)-AT-12, (e) Ti-MWW(P)-AT-16, (f) Ti-MWW(P)-AT-24.

**Table 1** Texture properties of the Ti-MWW(P)-AT-x.

View Article Online

DOI: 10.1039/D0CY00126K

Sample	Si/B <sup>a</sup>	Si/Ti <sup>a</sup>	Pore parameter <sup>b</sup>		
			S <sub>micro</sub>	V <sub>micro</sub>	V <sub>meso</sub>
Ti-MWW(P)-C	10	29	371	0.152	0.371
Ti-MWW(P)-AT-2	36	45	326	0.141	0.492
Ti-MWW(P)-AT-4	39	45	320	0.139	0.406
Ti-MWW(P)-AT-8	42	42	320	0.131	0.352
Ti-MWW(P)-AT-12	47	43	332	0.144	0.353
Ti-MWW(P)-AT-16	47	42	354	0.154	0.343
Ti-MWW(P)-AT-24	48	44	358	0.148	0.369

<sup>a</sup> Measured by ICP.

<sup>b</sup> Calculated by BET method and *t*-plot method. S<sub>micro</sub>(m<sup>2</sup>·g<sup>-1</sup>), V<sub>micro</sub>(cm<sup>3</sup>·g<sup>-1</sup>) and V<sub>meso</sub>(cm<sup>3</sup>·g<sup>-1</sup>) stand for the microporous surface area, microporous volume and mesoporous volume respectively.

spectra exhibit a major band at ca. 260 nm (Fig. 2A), and the only Raman band at 703 cm<sup>-1</sup> (Fig. 2B) emerges for Ti-MWW(P)-C sample. After the acid treatment, it could be observed that the 1446 cm<sup>-1</sup> band in Py-IR spectra recovers and the band intensity of 1540 cm<sup>-1</sup> decrease, which is a result of the removal of extraframework "TiO<sub>6</sub>" species and partial boron species (Fig. S3B and Table 1). Hence, the band at ca 230 nm in UV-Vis spectra and Raman band at ~1100 cm<sup>-1</sup> are exposed with Ti-MWW(P)-AT-24 (Fig. 2A and 2B). The high activity in the alkene epoxidation and cyclohexanone ammoximation for Ti-MWW(P)-AT-24 sample could further indicate the changes of active Ti species.(Fig. S4). In a summary, the state of Ti active species could influence significantly on the Lewis acidity and catalytic performance of Ti-MWW zeolite. Therefore, an in-depth survey of the changes of Ti species in Ti-MWW(P) during the acid treatment was carried out.

### 3.2 Changes of the Ti active species in Ti-MWW(P) sample during acid treatment

For gaining detailed information about the structure of Ti active species, the Ti-MWW(P)-AT-x samples were synthesized. The textural properties were confirmed, including the skeleton structure, porous uniformity and elementary compositions. There are faint distinctions in the XRD patterns and BET results (Fig. 3A and Table 1), which is indicative of the pure MWW phase and intact pore structure. The zeolite constituent was analysed by ICP measurements. It is observed that the atomic ratio of Si/Ti was maintained at the value of ~45, while the Si/B ratio increases gradually until reaching 48 (Table 1). This change is a result of the removal of extraframework "TiO<sub>6</sub>" and framework boron species from the Ti-MWW(P) sample. It is known that boron species could increase the electronegativity of skeleton, and thereby produce a negative effect on the catalytic ability of Ti active species<sup>26</sup>. Meanwhile, the synthesis

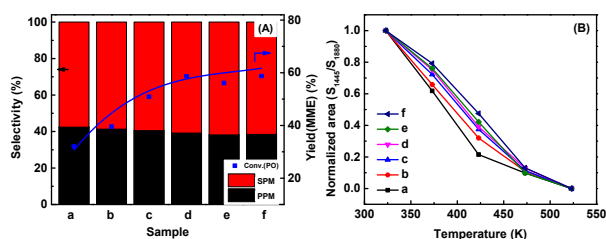


**Fig. 4** The ring-opening reaction of propylene oxide (PO) with  $\text{CH}_3\text{OH}$  over the Ti-MWW(P)-AT-x samples (A), and their normalized area in FT-IR spectra relative to Lewis acid sites ( $1446\text{ cm}^{-1}$ ) vs different evacuation temperatures (B): (a) Ti-MWW(P)-AT-2, (b) Ti-MWW(P)-AT-4, (c) Ti-MWW(P)-AT-8, (d) Ti-MWW(P)-AT-12, (e) Ti-MWW(P)-AT-16, (f) Ti-MWW(P)-AT-24. Reaction condition: catalyst, 100 mg; PO, 10 mmol;  $\text{CH}_3\text{OH}$ , 10 mL; temperature, 333 K; time, 120 min

of Ti-MWW zeolite involved the addition of boric acid and alkaline piperidine molecular<sup>13</sup>, which could stabilize the Si-O bond around the framework boron species, and therefore boron species in the Ti-MWW(P) are tetra-coordinated. As expected,  $^{11}\text{B}$  MAS NMR spectra shows a narrow band centred at the  $-2.2\text{ pm}$ , suggesting that the coordination of boron species (B(IV)) is saturated in Ti-MWW(P) (Fig. S5)<sup>58, 59</sup>. Hence, it was unable to remove completely all the boron species in Ti-MWW(P) only by prolonging treated time, because B(IV) species are hard to be extracted<sup>58, 60</sup>. Therefore, what's the effect of the twenty-four-hour acid treatment? The change of Ti active species in these Ti-MWW(P)-AT-x samples is tracked.

UV-Vis spectra of Ti-MWW(P)-AT-x samples are shown in Fig. 3B. It is observed that the intensity of the band at 230 nm is becoming stronger than that of the band at 210 nm as the time extends. The previous studies have suggested that at least five bands could be discerned by deconvolution, of which the band at 230 nm was assigned to the open  $\text{Ti}(\text{OSi})_3(\text{OH})$  species and that at 210 nm was considered as close  $\text{Ti}(\text{OSi})_4$  species<sup>11, 22, 35</sup>. After the peak fitting of the UV-Vis spectra (Fig. S6), the content of different Ti species in Ti-MWW(P)-AT-x samples could be analysed. Since the Si/Ti atomic ratio of the Ti-MWW(P)-AT-x samples is  $\sim 43$ , it could be deduced that the total content of  $\text{Ti}(\text{OSi})_3(\text{OH})$  species is increasing progressively. Meanwhile, a more obvious absorption band at  $3725\text{ cm}^{-1}$  was probed in the IR spectra (Fig. 3D), suggesting that the more Si-OH(Ti-OH) species were generated, which is in accordance with the UV-Vis measurements. In addition, the reaction involving the ring opening of propylene oxide (PO) with  $\text{CH}_3\text{OH}$  is considered as a typical probe reaction to determine the Si-OH(Ti-OH) species on titanosilicates.<sup>53</sup> Fig. 4A(a-f) shows that the conversion rate of PO increases gradually from 31.9% to 58.7%, and the ratio of 1-methoxy-2-propanol (PPM) to 2-methoxy-2-propanol (SPM) keeps at 40:60, which is a characteristic feature of Brønsted acid sites (such as ZSM-5 zeolite) catalyzing the PO ring-opening reactions<sup>53</sup>. Thus, it could be inferred that the more Si-OH(Ti-OH) species were formed with the acid-treated time lengthening. Moreover, UV-Raman technology was used for  $I_{554}/I_{348}$ , a symbol for the vibration intensity of "Ti-O-Si" bond in the MWW skeleton<sup>22</sup>, are observed (Fig. 3C). The declining trend indicates that the acid treatment accelerates the analysing the change of Ti species. The ratio of the  $I_{1096}/I_{348}$  and

**Table 2** Catalytic performance for the epoxidation of 1-hexene with  $\text{H}_2\text{O}_2$  Online  
DOI: 10.1039/D0CY00126K

Sample	Conv. (1-hex.)/% <sup>a</sup>	Conv. ( $\text{H}_2\text{O}_2$ )/% <sup>a</sup>	Eff. ( $\text{H}_2\text{O}_2$ )/% <sup>a</sup>	Sel. (Epo.)/% <sup>a</sup>	TON <sup>b</sup>
Ti-MWW(P)-AT-2	10.5	20.8	50.4	100.0	59
Ti-MWW(P)-AT-4	25.2	34.2	73.7	100.0	144
Ti-MWW(P)-AT-8	37.9	49.2	76.9	100.0	200
Ti-MWW(P)-AT-12	42.8	50.3	85.0	100.0	234
Ti-MWW(P)-AT-16	47.4	56.8	83.4	100.0	252
Ti-MWW(P)-AT-24	51.2	60.8	84.2	100.0	284

<sup>a</sup> Reaction conditions: catalyst 50 mg; 1-hexene 10 mmol;  $\text{H}_2\text{O}_2$  (30 wt.%) 10 mmol;  $\text{CH}_3\text{CN}$  10 mL; temp. 333 K; time 120 min. <sup>b</sup> In mol (mol.Ti)<sup>-1</sup>

formation of  $\text{Ti}(\text{OSi})_3(\text{OH})$  species via the cleavage of "Ti-O-Si" bond from the  $\text{Ti}(\text{OSi})_4$  species.

DFT theoretical calculations have suggested that Lewis-acid strength of  $\text{Ti}(\text{OSi})_3\text{OH}$  species was stronger than that of  $\text{Ti}(\text{OSi})_4$  species, that is, the more positive electrophilic ability of the Ti atoms in  $\text{Ti}(\text{OSi})_3\text{OH}$  species<sup>61, 62</sup>. Thus, Py-IR spectra of these Ti-MWW(P)-AT-x samples were exhibited in Fig. S7. The infrared bands, related to Lewis acidity, decrease sharply as evacuating temperature increases, whereas a weak band at  $1446\text{ cm}^{-1}$  can still be observed even the desorption temperature increases to 473 K. For a semi-quantity study of Lewis acid strength, the calculation for Lewis acid ( $1446\text{ cm}^{-1}$ ) was plotted as a function of evacuation temperature<sup>49, 57</sup>. In view of the holistic trend (Fig. 4B), it is clear that amounts of active centers with the strong acid property rises, as the treatment time went from 2 h to 24 h. After the above analysis, it is rational to hold the opinion that

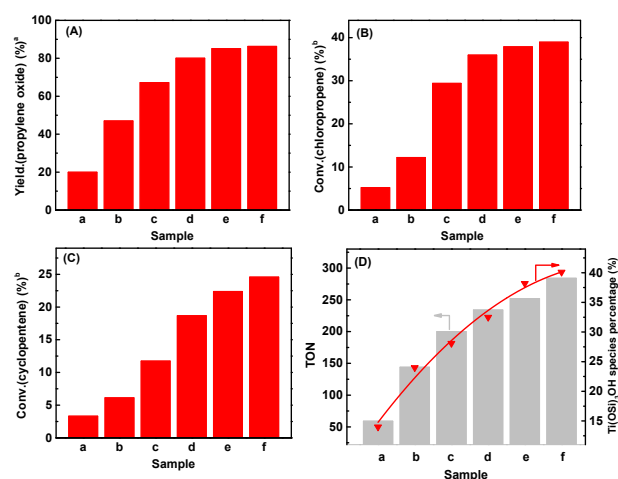


**Fig. 5** Catalytic reactions of different substrates over Ti-MWW(P)-AT-x zeolites: (A) the propylene, (B) the chloropropene, (C) the cyclopentene. And the correlation between the catalytic performance in 1-hexene epoxidation reaction and UV-Vis peak-fitting result (D). Samples are labeled as the following order: (a) Ti-MWW(P)-AT-2, (b) Ti-MWW(P)-AT-4, (c) Ti-MWW(P)-AT-8, (d) Ti-MWW(P)-AT-12, (e) Ti-MWW(P)-AT-16, (f) Ti-MWW(P)-AT-24. <sup>a</sup> Reaction conditions: catalyst 100 mg, propylene 30 mmol,  $\text{H}_2\text{O}_2$  (30 wt.%) 30 mmol,  $\text{CH}_3\text{CN}$  25 mL, temp 323 K, time 50 min. <sup>b</sup> Reaction conditions: catalyst 50 mg, chloropropene/cyclopentene 10 mmol,  $\text{H}_2\text{O}_2$  (30 wt.%) 10 mmol,  $\text{CH}_3\text{CN}$  10 mL, temp 333 K, time 120 min.

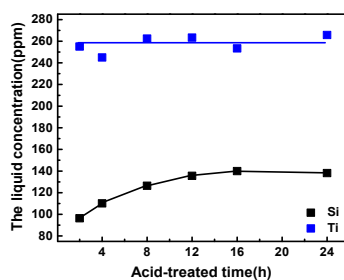


Fig. 6 The composition of the acid-treated solutions.

the longer the treatment time, the more  $\text{Ti}(\text{OSi})_3\text{OH}$  species produced in the process. The epoxidation of 1-hexene with  $\text{H}_2\text{O}_2$  was therefore adopted to exam the catalytic ability of the Ti-MWW(P)-AT-x samples. Surprisingly, it was found that the conversion of 1-hexene rose from 10.5% to 51.2% with the selectivity of epoxide at 100%, and the TON value of Ti species in Ti-MWW(P)-AT-24 arrived 284 (Table 2). The utilization efficiency of  $\text{H}_2\text{O}_2$  was also improved to ~85%, which could have a description of the high catalytic oxidation ability of these new active species. Besides, the versatile of  $\text{Ti}(\text{OSi})_3\text{OH}$  species is also examined in the epoxidation of propylene, chloropropene and cyclopentene, and the upward trend of conversion rate are also found (Fig. 5A-C). The concurrent linear dependence of the TON value in 1-hexene epoxidation and the amounts of  $\text{Ti}(\text{OSi})_3\text{OH}$  species on the acid-treated time was found (Fig. 5D), affirming the positive role of  $\text{Ti}(\text{OSi})_3\text{OH}$  species in catalytic performance.

It is reported that hydrophilicity/hydrophobicity has a significant effect on the catalytic performance of molecular sieves<sup>63-65</sup>, and therefore this character of Ti-MWW(P)-AT-x materials is measured by  $^{29}\text{Si}$  MAS NMR spectra (Fig. S8), which is regarded as a common method to detect the surface wettability of zeolites<sup>65-67</sup>. After the peak fitting of these spectra for Ti-MWW(P)-AT-x<sup>34</sup>, it could be observed that the ratio of the peak areas for the  $\text{Q}^2$  and  $\text{Q}^3$  sites to the sum of those for the  $\text{Q}^2$ ,  $\text{Q}^3$ , and  $\text{Q}^4$  sites increases obviously from Ti-MWW(P)-AT-2 to Ti-MWW(P)-AT-24, suggesting that more Si species in zeolites are functionalized by hydroxyl groups, and thereby the hydrophilicity of samples are enhanced. As it is known, the titanosilicates with more hydrophobic interior pores are active for the oxidation of alkanes and alkenes with aqueous  $\text{H}_2\text{O}_2$ , because of the improved mass transfer constraints<sup>63-65</sup>. Hence, the improved catalytic oxidation activity for Ti-MWW(P)-AT-x materials is not a result of the intensified hydrophilicity,

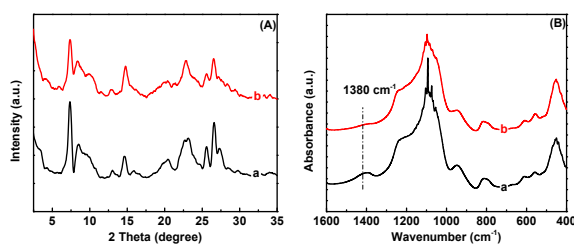


Fig. 7 Powder XRD patterns (A) and IR spectra (B) of Ti-MCM-56 (a) and Re-Ti-MCM-56(P)-AT-C (b).

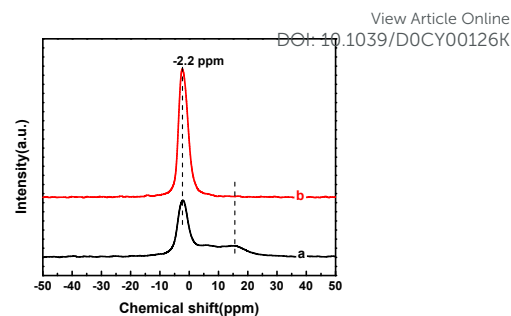


Fig. 8  $^{11}\text{B}$  MAS NMR spectra of the Ti-MCM-56 sample (a) and Re-Ti-MCM-56(P) sample (b).

Which may even play a negative role in various alkene epoxidation reactions. Meanwhile, the recent researches suggest that the presence of silanol nests ( $(\text{SiOH})_4$ ) in the vicinity of Ti active site impacts the thermodynamic activity of reagents and active intermediates at the active site, giving a large rise to the turnover rates for 1-octene epoxidation over the hydrophilic Ti-BEA<sup>30</sup>. For investigating the role of  $(\text{SiOH})_4$  groups in our materials, the  $\Phi_{\text{IR}}$  ( $A_{(\text{SiOH})_4}/A_{(\text{Si-O-Si})}$ )<sup>30</sup> are calculated for each Ti-MWW(P)-AT-x material through the deconvolution of the band ( $3500\text{ cm}^{-1}$ ) in IR spectra (Table S1). It is observed that although the value of  $\Phi_{\text{IR}}$  for each sample has a slight fluctuation, but it is almost in the range of 0.7~0.8, indicating that the number of silanol nests ( $(\text{SiOH})_4$ ) is almost equal in each Ti-MWW(P)-AT-x material.

After the above considerable discussions, it could be concluded competently that the newly-generated  $\text{Ti}(\text{OSi})_3\text{OH}$  is the most important factor for the improvement of catalytic performance in Ti-MWW(P)-AT-x samples. The catalytic cycles of Ti-MWW(P)-AT-24 were carried out in the 1-hexene epoxidation (Fig. S9). The catalyst was first reused after centrifugation and washing with acetone. The solid material was dried at  $80\text{ }^\circ\text{C}$  and then calcined at  $550\text{ }^\circ\text{C}$  for 6 h before the next run. After six runs, the 1-hexene conversion remains almost unchanged, showing that the catalyst is stable. The Ti-MWW(P)-AT-24 after reactions (named as Ti-MWW-U) was then analyzed by ICP, XRD, UV-Vis,  $^{29}\text{Si}$  MAS NMR and  $\text{N}_2$  adsorption-desorption measurements. Compared to the fresh Ti-MWW(P)-AT-24, the total Ti content of the Ti-MWW-U ( $\text{Si}/\text{Ti}=45$ ,  $\text{Si}/\text{B}=306$ ) remains almost unchanged, whereas the loss of boron species occurred. From the UV-Vis spectra (Fig. S10B), it could be observed that the fresh catalyst and Ti-MWW-U show the similar bands at 210 nm and 230 nm, suggesting that the framework Ti species is stable. The specific surface areas and microporous volumes of Ti-MWW-U is also measured to be  $346\text{ m}^2\cdot\text{g}^{-1}$  and  $0.150\text{ cm}^3\cdot\text{g}^{-1}$  respectively, suggesting that the porosity properties were not damaged. Meanwhile, no significant difference between the fresh catalyst and Ti-MWW-U was found in the XRD pattern and  $^{29}\text{Si}$  MAS NMR spectrum (Fig. S10A and C). After the careful evaluation of the catalyst, it is concluded that the Ti-MWW(P)-AT-24 has a good stability.

### 3.3 The evolution of titanium species in Ti-MWW sample

From the UV-Vis spectra in Fig. 3B(a), it is found that only a dominant absorption band at 210 nm is observed for the Ti-MWW(P)-AT-2 sample, meaning that interactions between the

**Table 3** Catalytic performance for the epoxidation of 1-hexene with H<sub>2</sub>O<sub>2</sub>

Sample	Si/Ti <sup>a</sup>	Si/B <sup>a</sup>	Conv. (1-hex.)/% <sup>b</sup>	Conv. (H <sub>2</sub> O <sub>2</sub> )/% <sup>b</sup>	Eff. (H <sub>2</sub> O <sub>2</sub> )/% <sup>b</sup>	Sel (Epo.)/% <sup>b</sup>	TON <sup>c</sup>
Ti-MCM-56	41	28	3.3	14.1	23.5	100.0	17
Ti-MCM-56-AT-C	56	69	6.1	15.9	38.2	100.0	42
Re-Ti-MCM-56(P) -AT-C	57	86	18.1	28.2	64.2	100.0	126

<sup>a</sup> Measured by ICP. <sup>b</sup> Reaction conditions: catalyst 50 mg; 1-hexene 10 mmol; H<sub>2</sub>O<sub>2</sub> (30 wt.%) 10 mmol; CH<sub>3</sub>CN 10 mL; temp. 333 K; time 120 min <sup>c</sup> In mol (mol.Ti)<sup>-1</sup>.

"TiO<sub>4</sub>" species and "TiO<sub>6</sub>" species are weak, and the latter species could be removed easily from Ti-MWW(P). Based on the preceding analysis, it is known that the band at 210 nm is assigned to perfect Ti(OSi)<sub>4</sub> species. As the acid-treated time extends, the transformation of the "TiO<sub>4</sub>" species from Ti(OSi)<sub>4</sub> to Ti(OSi)<sub>3</sub>OH could occur because of the increase of Ti(OSi)<sub>3</sub>OH species in Ti-MWW(P)-AT-x sample. Based on the steady Si/Ti ratio in zeolites and almost unchanged Ti contents (~260 ppm) in the acid-treated solutions (Fig. 6 and Table 1), there is less likely to happen that the extraframework "TiO<sub>6</sub>" species are inserted back in the framework and form the "TiO<sub>4</sub>" species. Meanwhile, the breaking of the "Ti-O-Si" bond from the Ti(OSi)<sub>4</sub> species could be confirmed by the decrease of band intensity at 554 and 1096 cm<sup>-1</sup> in UV-Raman spectra (Fig. 3C(a-f)). Thereafter, the continuous rise of Si content in acid-treated solutions, followed by the formation of Ti-related hydroxylation samples sites, is observed in this acid-treated process (Fig. 6 and Fig. S8), which could demonstrate that the Ti(OSi)<sub>3</sub>OH species originates from the conversion of Ti(OSi)<sub>4</sub> species.

For understanding the role of boron species in the acid-treated process, the Ti-MWW sample with the reserved boron species (Ti-MWW-(B)) has been prepared through the control of acid-treated condition. After the XRD and ICP measurements (Fig. S11 and Table S2), it was found that the Si/B of the Ti-MWW-(B) sample is lower than that of Ti-MWW(P)-AT-24 (17 vs 48), and the content of silicon species in the acid-treated solution is only ~100 ppm, which is also far lower than that in Ti-MWW(P)-AT-24 sample. Remarkably, the Ti-MWW-(B) sample shows a lower activity than that of Ti-MWW(P)-AT-24 in 1-hexene epoxidation reaction with the TON values being 284 to 82 (Table S2). The above comparisons indicate that the loss of silicon species is related to the removal of boron species, which could also affect the catalytic activity of zeolites. It is reported that the sitting of Ti atoms is adjacent to B atoms in the Ti-MCM-22 zeolite<sup>24,25</sup>, which could give us the hint about the structure of Ti species in Ti-MWW(P) sample. Based on the above description, it could be observed that the removal of boron species could result in the instability of the Si atom around Ti species, and promote the formation of new active Ti species. Thereby, the Scheme 1 could be put forward after the overall analysis of the relationship among the boron species, silicon species, and active Ti species.

Interestingly, it was found that the removal method of boron species also has a significant effect on the catalytic performance of molecular sieves. The research group<sup>58</sup> has suggested that stable silanol nests could only be generated when the

tetrahedral/saturated coordination boron species fell out. That means the extraction of B(IV) species is crucial for the shedding of Si species from Ti(OSi)<sub>4</sub> in our acidic environment. In order to verify this conjecture, the Ti-MCM-56 zeolite owning the peak at -2.2 ppm and a broad band at 10-17 ppm, attributed to the B(IV) species and B(III) species respectively<sup>59,60</sup> was employed. XRD patterns show the same topology structure for Re-Ti-MCM-56(P) and Ti-MCM-56 sample, whereas the different state of boron species is revealed by <sup>11</sup>B MAS NMR spectra (Fig. 7A and Fig. 8). Due to the existence of alkaline organic molecular (PI) in Re-Ti-MCM-56(P), the proton (H<sup>+</sup>) produced by the nearby B(IV) species could be compensated, and the bond Si-O-B in the tetrahedral [BO<sub>4</sub>] could be maintained<sup>68</sup>. The acid treatment is used to observe the effect of boron species on catalytic performance of the zeolites. Considering the weak band at 1380 cm<sup>-1</sup> in IR spectra, high Si/B ratio value in ICP measurement, and the low intensity of boron species in <sup>11</sup>B MAS NMR spectra, it is thought that the majority of boron species are removed (Fig. 7B, Table 3, and Fig. S12). Surprisingly, a great promotion of activity is found for the Re-Ti-MCM-56(P)-AT-C sample, with its TON value in 1-hexene epoxidation rising from 17 to 126, whereas the Ti-MCM-56-AT-C sample shows a little increase of reactivity (Table 3). Hence, it could be concluded that the removal of B(IV) species is a necessary part in the acid treatment.

In a summary (Scheme 1), it is believed that the acid treatment can improve the catalytic performance of MWW-type titanosilicate, which is through the removal of "BO<sub>4</sub>" species.

### 3.4 The effect of other factors on titanium species

Ti-MWW(P) with a different Si/Ti ratio (60) were also dealt with nitric acid. The three-dimensional MWW structure with high crystallinity is constructed within a short time (< 4 h) (Fig. S13A). It was observed that Ti-MWW(P)-AT-8 had almost the same catalytic reactivity than Ti-MWW(P)-AT-20, which may be due to the low Ti content in precursor (Si/Ti=60). Meanwhile, the intensity of absorption band at 230 nm in UV-Vis spectra also reaches the maximum when the acid-treated time arrives at 8 hours, which is accompanied by the improved TON value in 1-hexene reaction (Fig. S13B and Table S3).

Parameters of the acid-treated condition were also controlled to observe the effect on Ti-MWW(P) (Si/Ti=25). Extraframework titanium species are reserved when the acid concentration is 0.5 M, or the solid-to-liquid weight ratio remains at 1:20 (Fig. S14B(a) and Fig. S15B(a)), which is because this acidity is insufficient to wash them out. With the lift of the acid concentration or solid-to-liquid weight ratio, Ti(OSi)<sub>3</sub>OH species are formed gradually, followed by the increase of oxidation reactivity (Table S4 and Table S5). However, the loss of framework titanium species is unstoppable in a serious acidic environment (c(HNO<sub>3</sub>) > 2.5 M), decreasing the reactivity of catalyst (Table S4).

## 4. Conclusions

In this work, the comprehensive investigations about the active species in Ti-WWW zeolite were carried out. It is found that the catalytic ability depends on the state of active titanium species. The newly generated Ti(OSi)<sub>3</sub>OH species, with the strong Lewis-acid strength, take responsibility for the excellent performance in catalytic oxidation reactions. The formation process of Ti(OSi)<sub>3</sub>OH species was tracked. Results show that extra-framework "TiO<sub>6</sub>" species in Ti-MWW(P) can be removed easily. Extraction of B(IV) species could accelerate the shedding of vulnerable silicon species around the Ti(OSi)<sub>4</sub> species, thereby promoting the formation of efficient Ti(OSi)<sub>3</sub>OH species. Moreover, the catalytic performance of Ti-MCM-56 can also be improved with the removal of framework B(IV) species. Finally, this study could deepen the understanding of Ti active species in titanosilicate, and provide the researchers the facile strategy to design the other highly efficient catalysts

### Conflicts of interest

There are no conflicts to declare.

### Acknowledgements

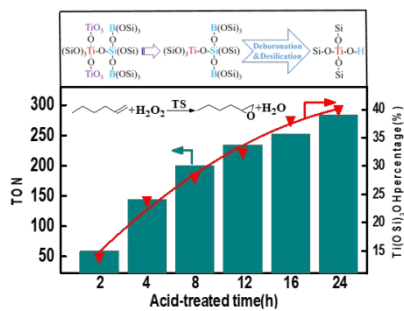
This work was supported by the National Natural Science Foundation of China (21673076), and the National Key Research and Development Program of China (2016YFB0701100).

### References

- M. He, Y. Sun and B. Han, *Angew. Chem. Int. Ed.*, 2013, **52**, 9620-9633.
- J. Přeck, *Cat. Rev.: Sci. Eng.*, 2018, **60**, 71-131.
- M. Sasaki, Y. Sato, Y. Tsuboi, S. Inagaki and Y. Kubota, *ACS Catal.*, 2014, **4**, 2653-2657.
- G. Wu, Y. Wang, L. Wang, W. Feng, H. Shi, Y. Lin, T. Zhang, X. Jin, S. Wang and X. Wu, *Chem. Eng. J.*, 2013, **215**, 306-314.
- X. Wang, M. Sun, B. Meng, N. Yang, S. Zhuang, X. Tan and S. Liu, *Chem. Eng. J.*, 2016, **289**, 494-501.
- H. Xu, Y. Zhang, H. Wu, Y. Liu, X. Li, J. Jiang, M. He and P. Wu, *J. Catal.*, 2011, **281**, 263-272.
- T. Blasco, M. Cambor, A. Corma, P. Esteve, J. Guil, A. Martinez, J. Perdigon-Melon and S. Valencia, *J. Phys. Chem. B*, 1998, **102**, 75-88.
- M. Liu, H. Wei, B. Li, L. Song, S. Zhao, C. Niu, C. Jia, X. Wang and Y. Wen, *Chem. Eng. J.*, 2018, **331**, 194-202.
- P. Wu, T. Tatsumi, T. Komatsu and T. Yashima, *Chem. Lett.*, 2000, **29**, 774-775.
- M. E. Leonowicz, J. A. Lawton, S. L. Lawton and M. K. Rubin, *science*, 1994, **264**, 1910-1913.
- P. Ratnasamy, D. Srinivas and H. Knozinger, *Adv. Catal.*, 2004, **48**, 1-169.
- Z. Zhuo, L. Wang, X. Zhang, L. Wu, Y. Liu and M. He, *J. Catal.*, 2015, **329**, 107-118.
- P. Wu, T. Tatsumi, T. Komatsu and T. Yashima, *J. Phys. Chem. B*, 2001, **105**, 2897-2905. DOI: 10.1039/D0CY00126K
- P. Wu, D. Nuntasri, Y. Liu, H. Wu, Y. Jiang, W. Fan, M. He and T. Tatsumi, *Catal. Today*, 2006, **117**, 199-205.
- X. Lu, Y. Guan, H. Xu, H. Wu and P. Wu, *Green Chem.*, 2017, **19**, 4871-4878.
- M. Pitínová-Šteková, P. Eliášová, T. Weissenberger, M. Shamzhy, Z. Musilová and J. Čejka, *Catal. Sci. Technol.*, 2018, **8**, 4690-4701.
- L. Xu, H.-g. Peng, K. Zhang, H. Wu, L. Chen, Y. Liu and P. Wu, *ACS Catal.*, 2012, **3**, 103-110.
- A. Corma, U. Díaz, V. Fornés, J. L. Jordá, M. Domine and F. Rey, *Chem. Commun.*, 1999, **9**, 779-780.
- R. Millini, G. Perego, W. Parker Jr, G. Bellussi and L. Carluccio, *Microporous Mater.*, 1995, **4**, 221-230.
- P. Wu, T. Miyaji, Y. Liu, M. He and T. Tatsumi, *Catal. Today*, 2005, **99**, 233-240.
- P. Wu and T. Tatsumi, *Chem. Commun.*, 2002, **10**, 1026-1027.
- S. Jin, Z. Wang, G. Tao, S. Zhang, W. Liu, W. Fu, B. Zhang, H. Sun, Y. Wang and W. Yang, *J. Catal.*, 2017, **353**, 305-314.
- S. Zhang, S. Jin, G. Tao, Z. Wang, W. Liu, Y. Chen, J. Luo, B. Zhang, H. Sun and Y. Wang, *Micro. Meso. Mater.*, 2017, **253**, 183-190.
- Y. Wang, D. Zhou, G. Yang, S. Miao, X. Liu and X. Bao, *J. Phys. Chem. A*, 2004, **108**, 6730-6734.
- D. Zhou, H. Zhang, J. Zhang, X. Sun, H. Li, N. He and W. Zhang, *Micro. Meso. Mater.*, 2014, **195**, 216-226.
- P. Wu, T. Tatsumi, T. Komatsu and T. Yashima, *J. Catal.*, 2001, **202**, 245-255.
- A. Corma, *Chem. Rev.*, 1995, **95**, 559-614.
- F. Qiu, X. Wang, X. Zhang, H. Liu, S. Liu and K. L. Yeung, *Chem. Eng. J.*, 2009, **147**, 316-322.
- N. s. A. Grosso-Giordano, C. Schroeder, A. Okrut, A. Solovyov, C. Schöttle, W. Chassé, N. a. Marinković, H. Koller, S. I. Zones and A. Katz, *J. Am. Chem. Soc.*, 2018, **140**, 4956-4960.
- D. T. Bregante, A. M. Johnson, A. Y. Patel, E. Z. Ayla, M. J. Cordon, B. C. Bukowski, J. Greeley, R. Gounder and D. W. Flaherty, *J. Am. Chem. Soc.*, 2019, **141**, 7302-7319.
- L. Wang, J. Sun, X. Meng, W. Zhang, J. Zhang, S. Pan, Z. Shen and F.-S. Xiao, *Chem. Commun.*, 2014, **50**, 2012-2014.
- M. Liu, Z. Xiao, J. Dai, W. Zhong, Q. Xu, L. Mao and D. Yin, *Chem. Eng. J.*, 2017, **313**, 1382-1395.
- D. T. Bregante and D. W. Flaherty, *ACS Catal.*, 2019, **9**, 10951-10962.
- X. Fang, Q. Wang, A. Zheng, Y. Liu, Y. Wang, X. Deng, H. Wu, F. Deng, M. He and P. Wu, *Catal. Sci. Technol.*, 2012, **2**, 2433-2435.
- L. Wu, Z. Tang, Y. Yu, X. Yao, W. Liu, L. Li, B. Yan, Y. Liu and M. He, *Chem. Commun.*, 2018, **54**, 6384-6387.
- L. Balducci, D. Bianchi, R. Bortolo, R. D'Aloisio, M. Ricci, R. Tassinari and R. Ungarelli, *Angew. Chem. Int. Ed.*, 2003, **42**, 4937-4940.
- Q. Guo, K. Sun, Z. Feng, G. Li, M. Guo, F. Fan and C. Li, *Chem. Eur. J.*, 2012, **18**, 13854-13860.
- L. Wu, X. Deng, S. Zhao, H. Yin, Z. Zhuo, X. Fang, Y. Liu and M. He, *Chem. Commun.*, 2016, **52**, 8679-8682.
- L. Wang, Y. Wang, Y. Liu, L. Chen, S. Cheng, G. Gao, M. He and P. Wu, *Micro. Meso. Mater.*, 2008, **113**, 435-444.
- M. A. Cambor, A. Corma, M.-J. Díaz-Cabañas and C. Baerlocher, *J. Phys. Chem. B*, 1998, **102**, 44-51.

41. Y. Zuo, M. Liu, T. Zhang, L. Hong, X. Guo, C. Song, Y. Chen, P. Zhu, C. Jaye and D. Fischer, *RSC Adv.*, 2015, **5**, 17897-17904.
42. L. Xu, D.-D. Huang, C.-G. Li, X. Ji, S. Jin, Z. Feng, F. Xia, X. Li, F. Fan and C. Li, *Chem. Commun.*, 2015, **51**, 9010-9013.
43. J. Su, G. Xiong, J. Zhou, W. Liu, D. Zhou, G. Wang, X. Wang and H. Guo, *J. Catal.*, 2012, **288**, 1-7.
44. C. E. Bamberger, G. M. Begun and C. S. MacDougall, *Appl. Spectrosc.*, 1990, **44**, 30-37.
45. Y. Su, M. L. Balmer and B. C. Bunker, *J. Phys. Chem. B*, 2000, **104**, 8160-8169.
46. J. Zhang, M. Li, Z. Feng, J. Chen and C. Li, *J. Phys. Chem. B*, 2006, **110**, 927-935.
47. X. Ji, L. Xu, X. Du, X. Lu, W. Lu, J. Sun and P. Wu, *Catal. Sci. Technol.*, 2017, **7**, 2874-2885.
48. G. A. Mekheimer, A. K. Nohman, N. E. Fouad and H. A. Khalaf, *Colloids Surf. A*, 2000, **161**, 439-446.
49. T. Barzetti, E. Selli, D. Moscotti and L. Forni, *J. Chem. Soc., Faraday Trans.*, 1996, **92**, 1401-1407.
50. W. Lin and H. Frei, *J. Am. Chem. Soc.*, 2002, **124**, 9292-9298.
51. W. Fan, P. Wu, S. Namba and T. Tatsumi, *J. Catal.*, 2006, **243**, 183-191.
52. Y. Wang, Y. Liu, X. Li, H. Wu, M. He and P. Wu, *J. Catal.*, 2009, **266**, 258-267.
53. L. Wu, S. Zhao, L. Lin, X. Fang, Y. Liu and M. He, *J. Catal.*, 2016, **337**, 248-259.
54. X. Lu, H. Xu, J. Yan, W.-J. Zhou, A. Liebens and P. Wu, *J. Catal.*, 2018, **358**, 89-99.
55. M. Hunger, S. Ernst and J. Weitkamp, *Zeolites*, 1995, **15**, 188-192.
56. M. A. Cambor, C. Corell, A. Corma, M.-J. Díaz-Cabañas, S. Nicolopoulos, J. M. González-Calbet and M. Vallet-Regí, *Chem. Mater.*, 1996, **8**, 2415-2417.
57. S. Zhao, D. Yang, X. Zhang, X. Yao, Y. Liu and M. He, *Chem. Commun.*, 2016, **52**, 11191-11194.
58. R. De Ruiter, A. Kentgens, J. Grootendorst, J. Jansen and H. Van Bekkum, *Zeolites*, 1993, **13**, 128-138.
59. J. Chen, T. Liang, J. Li, S. Wang, Z. Qin, P. Wang, L. Huang, W. Fan and J. Wang, *ACS Catal.*, 2016, **6**, 2299-2313.
60. A. Hough, A. F. Routh, S. M. Clarke, P. V. Wiper, J. A. Amelse and L. Mafra, *J. Catal.*, 2016, **334**, 14-22.
61. B. D. Montejo-Valencia, J. L. Salcedo-Pérez and M. C. Curet-Arana, *J. Phys. Chem. C*, 2016, **120**, 2176-2186.
62. D. H. Wells Jr, W. N. Delgass Jr and K. T. Thomson, *J. Am. Chem. Soc.*, 2004, **126**, 2956-2962.
63. C. Khouw, C. Dartt, J. Labinger and M. Davis, *J. Catal.*, 1994, **149**, 195-205.
64. A. Corma, P. Esteve and A. Martínez, *J. Catal.*, 1996, **161**, 11-19.
65. L. Wang, Y. Liu, W. Xie, H. Wu, X. Li, M. He and P. Wu, *J. Phys. Chem. C*, 2008, **112**, 6132-6138.
66. L. Wang, J. Sun, X. Meng, W. Zhang, J. Zhang, S. Pan, Z. Shen and F.-S. Xiao, *Chem. Commun.*, 2014, **50**, 2012-2014.
67. X. Lu, W.-J. Zhou, Y. Guan, A. Liebens and P. Wu, *Catal. Sci. Technol.*, 2017, **7**, 2624-2631.
68. V. R. Marthala, W. Wang, J. Jiao, Y. Jiang, J. Huang and M. Hunger, *Micro. Meso. Mater.*, 2007, **99**, 91-97.

View Article Online  
DOI: 10.1039/D0CY00126K



Regulating the state of titanium species via the deboronation-assisted route is a facile strategy to construct the highly efficient titanosilicate catalysts.